Temporal and spatial characteristics of ozone depletion events from measurements in the Arctic

J. W. Halfacre[1], T. N. Knepp[1,*], P. B Shepson[1,2], C. R. Stephens[1,], K. A. Pratt[1,***], B. Li[3,****], P. K. Peterson[4], S. J. Walsh[4], W. R. Simpson[4], P. A. Matrai[5], J. W. Bottenheim[6], S. Netcheva[7], D. K. Perovich[8], A. Richter[9]**

[1]{Department of Chemistry, Purdue University, West Lafayette, Indiana, USA}

[2]{Department of Earth, Atmospheric, and Planetary Sciences, Purdue University, West Lafayette, Indiana, USA}

[3]{Department of Statistics, Purdue University, West Lafayette, Indiana, USA}

[4]{Department of Chemistry, University of Alaska, Fairbanks, Alaska, USA}

[5]{Bigelow Laboratory for Ocean Sciences, East Boothbay, Maine, USA}

[6]{Air Quality Research Division, Environment Canada, Toronto, Ontario, Canada}

[7]{Air Quality Processes Research Section, Environment Canada, Toronto, Ontario, Canada}

[8]{U.S. Army Cold Regions Research and Engineering Laboratory, Fairbanks, Alaska, USA}

[9]{Institute of Environmental Physics, University of Bremen, Bremen, Germany}

[*]{now at Science Systems and Applications, Inc., Hampton, Virginia, USA}

[**]{now at Institute of Arctic and Alpine Research, University of Colorado at Boulder, Boulder, Colorado, USA}

[***]{now at Department of Chemistry, University of Michigan, Ann Arbor, Michigan, USA}

[****]{now at Department of Statistics, University Illinois at Urbana-Champaign, Urbana, Illinois, USA}

Correspondence to: J. W. Halfacre (jhalfacr@purdue.edu)

2.3 Air Mass Trajectory Analysis

As discussed in Sect. 2.3, the NOAA HYSPLIT air mass trajectory model was used to estimate the spatial scales of ODEs and some meteorological parameters (i.e. temperature and wind speed). In obtaining the back trajectories, the time lengths for which the back trajectories were run were determined by the temporal lengths of the ODEs themselves. This time length was defined as the time between the ODE start time and the O_3-decrease stop time. A distribution of the time scale for each ODE is presented in Fig. S1. Though there is a large level of uncertainty associated with using a back trajectory model for longer than more than a few days (Kahl, 1993), we see the majority of events occur on a timescale of less than 4 days.

2.4 Monte Carlo Experiment

Two versions of a Monte Carlo experiments were performed to determine the statistical probability of overlap of O_3-depleted air masses with O-Buoys locations. In the first, 17 different sized, circular air masses, determined by the spatial scale estimations of ODEs determined by O-Buoys placed in the Arctic Ocean (O-Buoys1 and 2; Fig. S2) were randomly placed in an area defined by the bounds of the sea ice in the Arctic Ocean.

3.1 Ozone Depletion Timescale

The amount of MAX-DOAS data available during the 2009 deployment of O-Buoy1 in Barrow was limited by the amount of solar radiation present. The solar elevation angle remained low enough such that there can exist substantial gaps between subsequent periods of BrO measurements. In spite of these gaps, the average BrO mole fractions during three ODEs were comparable to the calculated BrO required for the observed ozone depletion timescale (Table S1), and are discussed below.

In the events starting 30 Mar 2009 (Fig. S3a) and 12 Apr 2009 (Fig. S3b), O_3 levels can be seen to decrease as BrO begins to rise before the several hour BrO data gaps. As can be seen from Table S1, the average BrO observed during this period was 8.5 pmol mol^{-1} and 13.0 pmol mol^{-1} for 30 Mar and 12 Apr, respectively, while the observed rate of O_3 depletion was calculated to require 9.6 pmol mol^{-1} and 4.2 pmol mol^{-1}, respectively. The 30 Mar event occurred with relatively steady winds (between 6 and 8 m s^{-1}), while the 12 Apr event wind speeds gradually fell from 10 m s^{-1}. Both events occurred under fairly steady temperatures. The third event (02 May 2009) required 16.1 pmol mol^{-1} BrO, while the observed BrO was 13.1 pmol mol^{-1}. This event also occurred under steadily decreasing temperatures and calm winds ($\leq$5 m s^{-1}; Fig. S3c). While there are no BrO data at the onset of O_3 depletion, there was a noticeable increase in BrO levels in the mid afternoon. Forty-eight hour HYSPLIT backward trajectories (Draxler, 1999) were computed every 2 hours during the period of O_3 decrease, starting from the O_3 decrease stop time (Fig. S3d,e, f). For the 30 Mar and 12 Apr events, the trajectories agreed that the air masses travel near the coast of the Canadian archipelago, an area for which satellites have observed enhanced BrO (Choi et al., 2012; Koo et al., 2012; Richter et al., 1998; Salawitch et al., 2010). The trajectories during the 02 May O_3 decrease showed that air had traveled from across the sea ice in the Beaufort and Chuckchi Seas.

It would be expected that Barrow, a coastal location, would observe ODEs primarily due to the advection of O_3 depleted air, given the evolution of the solar elevation angle during polar spring and findings from previous studies (Bottenheim and Chan, 2006; Koo et al., 2012; Oltmans et al., 2012). The observations here are not inconsistent with these ODEs initiating locally relative to the O-Buoy given the presence of BrO; in the absence of O_3, the lifetime of BrO is controlled by its photolysis, which is about 100 seconds (Lehrer et al., 2004; Simpson et al., 2007), and thus observations of local BrO in the boundary layer should be indicative of active O_3 destruction chemistry. However, the gaps in the BrO data prevent us from making any further conclusions.

3.2 ODE spatial scales

To estimate how many buoys would be required for consistent overlap of ODE sizes with the site of O-Buoys, we repeated the Monte Carlo experiments with two additional observation points at potential sites of future O-Buoys for a total of three observation sites. The first is near the North Pole (86˚N, 54˚W), an area that has been previously shown to feature deep, long-term depletions of O_3 (Bottenheim et al., 2009). The second is in the East Siberian Sea (75˚N, 170˚E), which is in an area that back trajectory studies have shown O_3-poor air to originate. Figure S4 shows that, with the three simultaneously observation points, the mode of the frequency vs. number of overlaps plot shift to 5, instead of 0 using just one observation site (Fig. 9a). Additionally, there are no instances of the experiment in which the 17 ODEs sizes from the distribution did not overlap with an O-Buoy.

3.3 Temperature and wind speed during ODEs

To determine whether the wind speeds observed during ODEs had some relation to ODEs, we also examined the wind speeds during times when ozone was not depleted (non-ODEs). In the case of wind speeds observed by the O-Buoys, the majority of wind speeds are between 1-4 m s^{-1} during non-ODEs (Fig. S5a) with a clear mode at 3.5 m s^{-1} (median ~3.9 m s^{-1}). As a comparison, the wind speeds during the ODE cases typically range between 2-5 m s^{-1} with a mode of 3.5 m s^{-1} and median of ~3.6 m s^{-1} (Fig 12a). To determine whether wind speeds upwind were different than those measured at the buoy, we calculated average wind speeds for each non-ODE from the HYSPLIT backward air mass trajectories (Draxler and Hess, 1997, 1998; Draxler, 1999) by dividing the length of each trajectory by the time span of the ODE (ODE start time – ODE end time). The HYSPLIT analysis for the non-ODE cases showed a mode comparable to the ODE case at 3.5 m s^{-1} (median 5 m s^{-1}) with 21 of 33 cases between 5 and 6 m s^{-1} (Fig. S5b). These results do not show a clear difference between wind speeds occurring during ODEs and those occurring during non-ODEs.

References

Bottenheim, J. W., and Chan, E.: A trajectory study into the origin of spring time Arctic boundary layer ozone depletion, J. Geophys. Res., 111, D19301, doi:10.1029/2006jd007055, 2006.

Bottenheim, J. W., Netcheva, S., Morin, S., and Nghiem, S. V.: Ozone in the boundary layer air over the Arctic Ocean: measurements during the TARA transpolar drift 2006-2008, Atmos. Chem. Phys., 9, 4545-4557, 2009.

Choi, S., Wang, Y., Salawitch, R. J., Canty, T., Joiner, J., Zeng, T., Kurosu, T. P., Chance, K., Richter, A., Huey, L. G., Liao, J., Neuman, J. A., Nowak, J. B., Dibb, J. E., Weinheimer, A. J., Diskin, G., Ryerson, T. B., da Silva, A., Curry, J., Kinnison, D., Tilmes, S., and Levelt, P. F.: Analysis of satellite-derived Arctic tropospheric BrO columns in conjunction with aircraft measurements during ARCTAS and ARCPAC, Atmos. Chem. Phys., 12, 1255-1285, doi:10.5194/Acp-12-1255-2012, 2012.

Draxler, R. R., and Hess, G. D.: Description of the HYSPLIT 4 modeling system. NOAA Tech. Memo. ERL ARL-224, NOAA Air Resources Laboratory, Silver Spring, MD, 1997.

Draxler, R. R., and Hess, G. D.: An overview of the HYSPLIT 4 modeling system of trajectories, dispersion, and deposition, Aust. Meteor. Mag., 47, 295-308, 1998.

Draxler, R. R.: HYSPLIT 4 users's guide, U.S. Dept. of Commerce, National Oceanic and Atmospheric Administration, Environmental Research Laboratories, Air Resources Laboratory, Silver Spring, Md., 1999.

Kahl, J. D.: A Cautionary Note on the Use of Air Trajectories in Interpreting Atmospheric Chemistry Measurements, Atmos. Environ., Part A, 27, 3037-3038, 1993.

Koo, J. H., Wang, Y., Kurosu, T. P., Chance, K., Rozanov, A., Richter, A., Oltmans, S. J., Thompson, A. M., Hair, J. W., Fenn, M. A., Weinheimer, A. J., Ryerson, T. B., Solberg, S., Huey, L. G., Liao, J., Dibb, J. E., Neuman, J. A., Nowak, J. B., Pierce, R. B., Natarajan, M., and Al-Saadi, J.: Characteristics of tropospheric ozone depletion events in the Arctic spring: analysis of the ARCTAS, ARCPAC, and ARCIONS measurements and satellite BrO observations, Atmos. Chem. Phys., 12, 9909-9922, doi:10.5194/Acp-12-9909-2012, 2012.

Lehrer, E., Hönninger, G., and Platt, U.: A one dimensional model study of the mechanism of halogen liberation and vertical transport in the polar troposphere, Atmos. Chem. Phys., 4, 2427-2440, 2004.

Oltmans, S. J., Johnson, B. J., and Harris, J. M.: Springtime boundary layer ozone depletion at Barrow, Alaska: Meteorological influence, year-to-year variation, and long-term change, J. Geophys. Res., 117, doi:10.1029/2011jd016889, 2012.

Richter, A., Wittrock, F., Eisinger, M., and Burrows, J. P.: GOME observations of tropospheric BrO in northern hemispheric spring and summer 1997, Geophys. Res. Lett., 25, 2683-2686, 1998.

Salawitch, R. J., Canty, T., Kurosu, T., Chance, K., Liang, Q., da Silva, A., Pawson, S., Nielsen, J. E., Rodriguez, J. M., Bhartia, P. K., Liu, X., Huey, L. G., Liao, J., Stickel, R. E., Tanner, D. J., Dibb, J. E., Simpson, W. R., Donohoue, D., Weinheimer, A., Flocke, F., Knapp, D., Montzka, D., Neuman, J. A., Nowak, J. B., Ryerson, T. B., Oltmans, S., Blake, D. R., Atlas, E. L., Kinnison, D. E., Tilmes, S., Pan, L. L., Hendrick, F., Van Roozendael, M., Kreher, K., Johnston, P. V., Gao, R. S., Johnson, B., Bui, T. P., Chen, G., Pierce, R. B., Crawford, J. H., and Jacob, D. J.: A new interpretation of total column BrO during Arctic spring, Geophys. Res. Lett., 37, L21805, doi:10.1029/2010GL043798, 2010.

Simpson, W. R., von Glasow, R., Riedel, K., Anderson, P., Ariya, P., Bottenheim, J., Burrows, J., Carpenter, L. J., Frieß, U., Goodsite, M. E., Heard, D., Hutterli, M., Jacobi, H. W., Kaleschke, L., Neff, B., Plane, J., Platt, U., Richter, A., Roscoe, H., Sander, R., Shepson, P., Sodeau, J., Steffen, A., Wagner, T., and Wolff, E.: Halogens and their role in polar boundary-layer ozone depletion, Atmos. Chem. Phys., 7, 4375-4418, 2007.

Table S1: Average BrO mole fractions during periods of O_3 decrease from O-Buoy1 at Barrow, AK, MAX-DOAS, the corresponding propagated errors, and the estimated BrO required for the observed O_3 depletion timescales based on Eq. 5 (Sect. 3.1 of the main text).

ODE start time (UTC)	O_3 decrease stop time (UTC)	Observed τ_{O_3} (hours)	Average observed BrO (pmol mol^{-1})	Measurement uncertainty (pmol mol^{-1})	Estimated BrO required from observed τ_{O_3} (pmol mol^{-1})
30 Mar 2009 20:06	31 Mar 2009 19:20	24.3	8.5	3.2	9.6
12 Apr 2009 06:18	14 Apr 2009 11:22	71.7	13.0	3.2	4.2
02 May 2009 05:51	02 May 2009 23:00	18.7	13.1	3.0	16.1

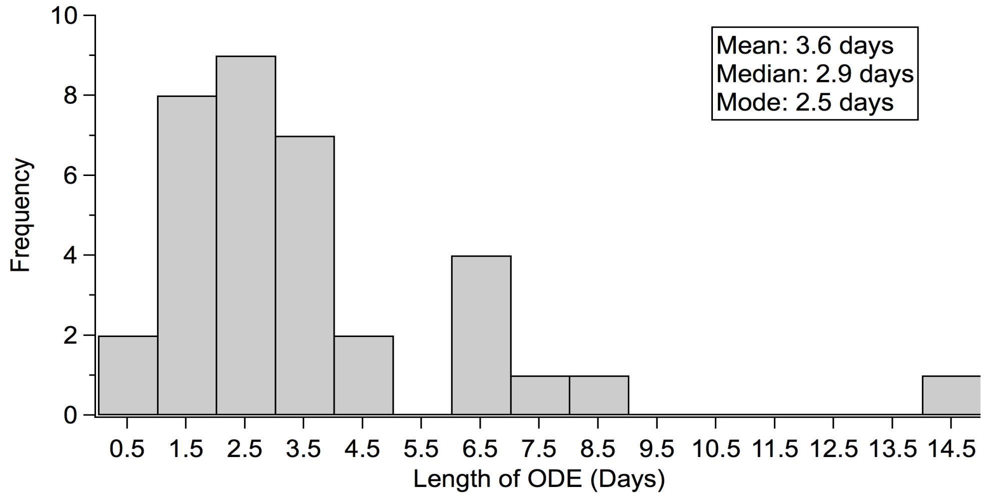

Figure S1: Time lengths of ODEs as defined by the ODE start time and the O_3 decrease stop time.

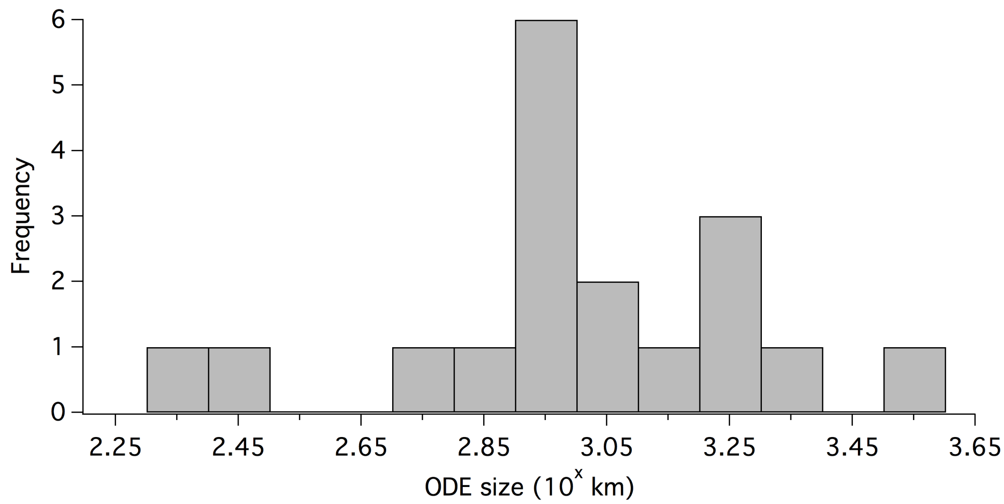

Figure S2: Distribution of ODE sizes utilized in the Monte Carlo experiments. These 17 sizes come from O_3 data observed from O-Buoy1 and O-Buoy2.

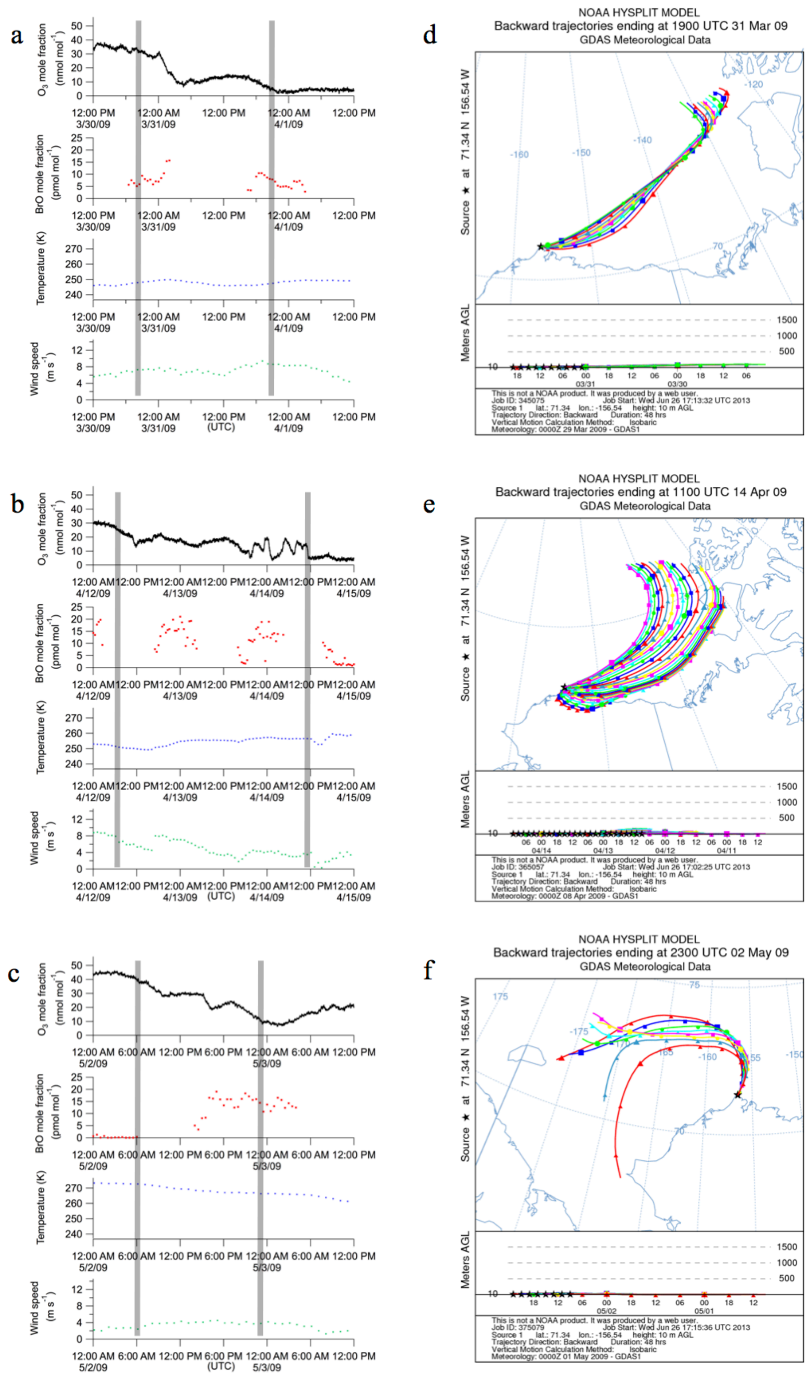

Figure S3: Periods of O_3 decrease from O-Buoy1 at Barrow and corresponding 48 hour HYSPLIT backward trajectories (computed every two hours during these time periods). Decrease starts at a, b) 20:06 30 Mar 2009; c, d) 06:18 12 Apr 2009; and e, f) 05:51 02 May 2009. Transparent black bars represent the ODE start time and O_3 decrease stop time as defined in Sect. 2.2.

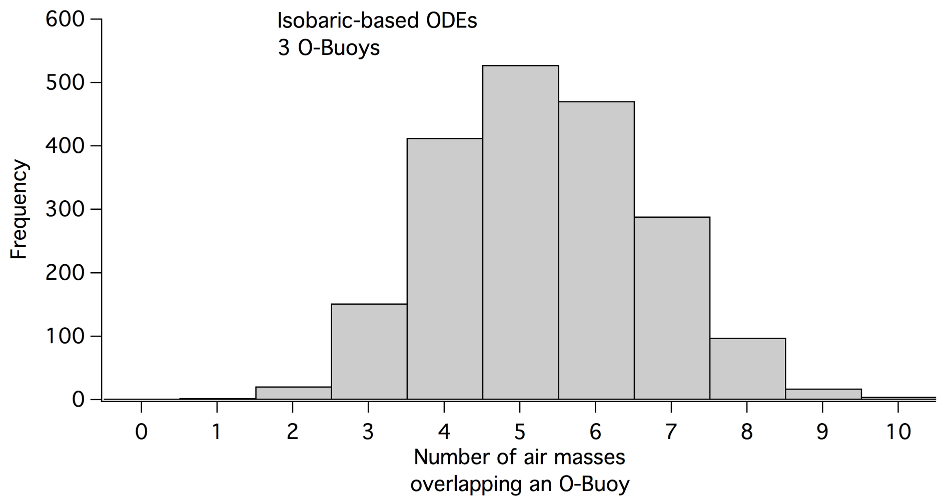

Figure S4: Results from Monte Carlo simulation experiment with three observation sites. Histogram shows the number of times a circular air mass overlapped with at least one observation site out of 2000 iterations.

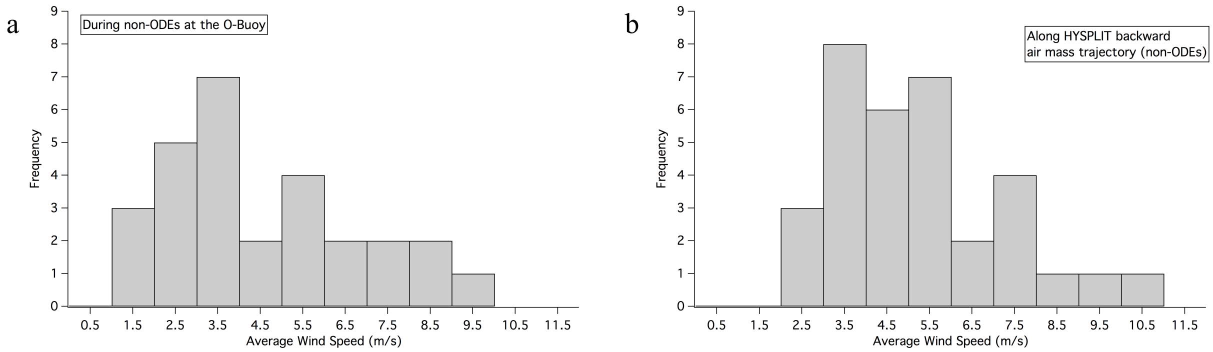

Figure S5: a) Histogram of the average wind speed measured by the O-Buoys during non-ODEs. b) Histogram of average wind speeds from non-ODEs, as determined from the HYSPLIT backward air mass trajectory.